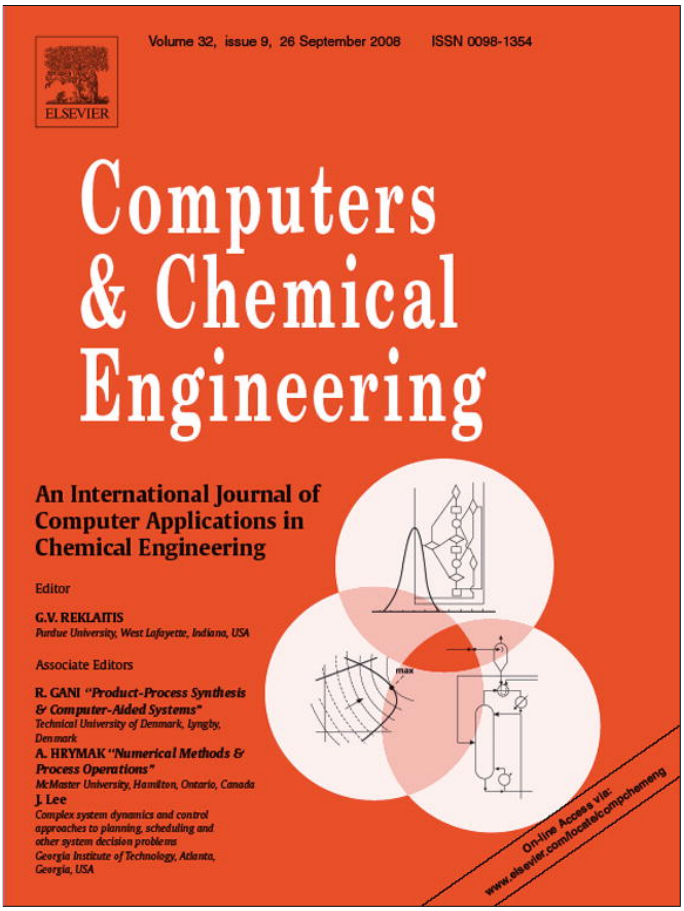

Available online at www.sciencedirect.com
ScienceDirect
Computers and Chemical Engineering 32 (2008) 2123–2135
Computers & Chemical Engineering
www.elsevier.com/locate/compchemeng

Optimal control of diffusion-convection-reaction processes using reduced-order models

Mingheng Li [a], Panagiotis D. Christofides [b,*]

[a] Department of Chemical and Materials Engineering, California State Polytechnic University, Pomona, CA 91768, United States
[b] Department of Chemical and Biomolecular Engineering, University of California, Los Angeles, CA 90095-1592, United States

Received 24 July 2007; received in revised form 26 October 2007; accepted 26 October 2007
Available online 4 November 2007

Abstract

Two approaches for optimal control of diffusion-convection-reaction processes based on reduced-order models are presented. The approaches differ in the way spatial discretization is carried out to compute a reduced-order model suitable for controller design. In the first approach, the partial differential equation (PDE) that describes the process is first discretized in space and time using the finite difference method to derive a large number of recursive algebraic equations, which are written in the form of a discrete-time state-space model with sparse state, input and output matrices. Snapshots based on this high-dimensional state-space model are generated to calculate empirical eigenfunctions using proper orthogonal decomposition. The Galerkin projection with the computed empirical eigenfunctions as basis functions is then directly applied to the high-dimensional state-space model to derive a reduced-order model. In the second approach, a continuous-time finite-dimensional state-space model is constructed directly from the PDE through application of orthogonal collocation on finite elements in the spatial domain. The dimension of the derived state-space model can be further reduced using standard model reduction techniques. In both cases, optimal controllers are designed based on the low-order state-space models using discrete-time and continuous-time linear quadratic regulator (LQR) techniques. The effectiveness of the proposed methods are illustrated through applications to a diffusion-convection process and a diffusion-convection-reaction process.

Keywords: Optimal control; Diffusion-convection-reaction processes; Model reduction; Empirical eigenfunctions; Orthogonal collocation

1. Introduction

Distributed chemical processes are naturally described by partial differential equations (PDEs) that are able to describe the spatiotemporal evolution of the process dynamics. Representative examples include chemical vapor deposition of semiconductor materials (Armaou & Christofides, 1999; Li, Sopko, & McCamy, 2006; Lin & Adomaitis, 2001; Theodoropoulou, Adomaitis, & Zafiriou, 1998), thermal spray processing of coatings (Li & Christofides, 2005, 2006) and fluid flows (Baker, Armaou, & Christofides, 2000; Graham, Peraire, & Tang, 1999; Park & Jang, 2000; Rowley, Colonius, & Murray, 2004). In order to develop accurate numerical solutions, the PDEs are usually converted to and solved as ordinary differential equations (ODEs) or algebraic equations using numerical methods like finite element and finite volume, etc. (e.g. Ammar, Ryckelynck, Chinesta, & Keunings, 2006; Broussely, Bertin, & Lagonotte, 2003; Kalkkuhl & Doring, 1993; Liu & Jacobsen, 2004). Generally speaking, the resulting state-space model is of high dimension in order to precisely describe the spatial characteristics, especially when sharp gradients exist in the spatial domain. In order to develop dynamic optimization algorithms or feedback control systems suitable for real-time implementation, advanced model reduction techniques such as Galerkin projection with empirical eigenfunctions, combination of Galerkin's method with approximate inertial manifolds, Krylov subspace and balanced truncation have been proposed to derive low-order ODEs with reasonable accuracy (Armaou & Christofides, 1999, 2000, 2002; Baker & Christofides, 2000; Baker et al., 2000; Bendersky & Christofides, 2000; Christofides, 2001; Christofides & Daoutidis, 1997; Park & Jang, 2000; Rowley et al., 2004; Shvartsman & Kevrekidis, 1998). The controller is

* Corresponding author.
E-mail addresses: minghengli@csupomona.edu (M. Li), pdc@seas.ucla.edu (P.D. Christofides).

0098-1354/$ – see front matter © 2007 Elsevier Ltd. All rights reserved.
doi:10.1016/j.compchemeng.2007.10.018

then designed based on the reduced-order models, resulting in a significant reduction in the time needed to compute the control action.

In this work, we will present two optimal control approaches for diffusion-convection-reaction processes using reduced-order models. In the first approach, the finite difference method is initially used and the PDE is converted to a large number of recursive algebraic equations. These algebraic equations are written in the form of discrete-time state-space models with sparse state, input and output matrices. Subsequently, snapshots based on the high-dimensional state-space model are generated to calculate empirical eigenfunctions using proper orthogonal decomposition. The Galerkin projection with the empirical eigenfunctions as basis functions is then directly applied to the high-dimensional state-space model to derive a low-order discrete-time state-space model. In the second approach, the finite-element based orthogonal collocation is used. In this case, a number of high-order Lagrange interpolation polynomials are applied on a finite number of collocation elements in the spatial domain to directly derive a low-dimensional differential-algebraic equation (DAE) model (Quarteroni & Valli, 1997). Such a DAE can be converted to a continuous-time state-space model by incorporating the boundary conditions into the ODEs in the spatial domain. If necessary and the properties of the resulting ODE system allow, the dimension of the derived state-space model can be further reduced using model reduction techniques based on time-scale decomposition arguments. In either case, the optimal control laws are designed based on the low-dimensional state-space models or their linearized forms using discrete-time or continuous-time linear quadratic regulator (LQR) control techniques.

The proposed methods are applied to two concentration transition problems in an isothermal dispersed tubular reactor. The concentration transition problem is an important subject at the interface of reactor engineering and process control. This type of problem arises in modern chemical plants which generally make various products that differ in composition only in order to satisfy the needs of different customers. Representative industrial examples include grade transition in a polyethylene plant (e.g. Cervantes, Tonelli, Brandolin, Bandoni, & Biegler, 2002; Lo & Ray, 2006; McAuley & MacGregor, 1992) and colored glass product transition in a glass plant (e.g. Trier, 1987). In certain circumstances, a product transition may take days or weeks if the reactor is huge and the residence time of the reactor is large. A reduction of the transition time, which can be solved as an optimal control problem, can bring about significant economic benefits (Li & Christofides, 2007). In this work, we will focus on a type of concentration transition problem in which the grade of the final product is regulated through the concentration of a key component that is fed at the entrance of the reactor, e.g. the transition of one colored glass product to another by regulating the colorant agent (key component) in the batch material which is then incorporated in the glass melt before exiting (Trier, 1987). If the key component to be controlled is not involved in any reactions, the transition process is described as a diffusion-convection process. If it does participate in any reaction, the process is a diffusion-convection-reaction process. In the remainder, we first focus on a diffusion-convection process and design an optimal controller on the basis of a reduced-order model constructed through Galerkin projection with empirical eigenfunctions as basis functions. Subsequently, we focus on a diffusion-convection-reaction process and design an optimal controller on the basis of a reduced-order model constructed through orthogonal collocation.

2. Optimal control of diffusion-convection processes

2.1. Control problem formulation

In this section, we focus on an isothermal dispersed tubular reactor in which the key component concentration is described by a parabolic PDE subject to the so-called Danckwerts boundary conditions (Danckwerts, 1953):

$$\frac{\partial U(z,t)}{\partial t} = -v\frac{\partial U(z,t)}{\partial z} + D\frac{\partial^2 U(z,t)}{\partial z^2}, \qquad \text{s.t.}$$
$$vU(0^-,t) = vU(0^+,t) - D\left.\frac{\partial U(z,t)}{\partial z}\right|_{z=0^+}, \quad \left.\frac{\partial U(z,t)}{\partial z}\right|_{z=L} = 0 \tag{1}$$

where $U(0^-,t) = u(t)$ is the inlet concentration (input variable), $U(L,t) = y(t)$ is the outlet concentration (output variable), t is the time, v is the fluid velocity in the reactor, L is the length of the reactor and D is the diffusion coefficient (or, more generally, dispersion coefficient). The control problem is to minimize the following functional:

$$\min_{u(t)} J = \int_0^\infty (y(t) - y_f)^2\,\mathrm{d}t + \epsilon^2 \int_0^\infty (u(t) - u_f)^2\,\mathrm{d}t \tag{2}$$

subject to the process dynamics described in Eq. (1), where u_f and y_f are the steady-state concentration of the key component at the inlet and outlet of the reactor after transition, and ϵ represents the weight on the control action during the transition process. Due to the linear nature of the process and the fact that all the molecules fed to the process will eventually flow out, the concentration transition problem can be converted to a dimensionless form in which the dimensionless concentration before and after transition is 0 and 1, respectively (Li & Christofides, 2007).

2.2. Spatial and temporal discretization of the PDE model

We first employ a standard finite difference discretization of the PDE of Eq. (1) in both time and space to obtain an accurate solution. Specifically, using the explicit finite difference approach with the forward time and center space (FTCS) scheme, the PDE of Eq. (1) can be written as the following set of algebraic equations:

$$\frac{U(z_i,t_{j+1}) - U(z_i,t_j)}{\Delta t} = -v\frac{U(z_{i+1},t_j) - U(z_{i-1},t_j)}{2\Delta z}$$

$$+ D\frac{U(z_{i+1},t_j) - 2U(z_i,t_j) + U(z_{i-1},t_j)}{(\Delta z)^2},$$

$$i = 1,\ldots,N+1;\quad vU(z_1,t_j) = vu + D\frac{U(z_2,t_j) - U(z_0,t_j)}{2\Delta z},$$

$$0 = D\frac{U(z_{N+2},t_j) - U(z_N,t_j)}{2\Delta z} \tag{3}$$

where $N+1$ is the total number of nodes in the spatial domain (with nodes 1 and $N+1$ represent the left and right boundaries), and i and j are the spatial and temporal indices, respectively. Note that two fictitious points (z_0 and z_{N+2}) are used to approximate $\partial U/\partial z$ on the boundaries. The values of the variable at these fictitious points can be expressed through boundary conditions as

$$U(z_0,t_j) = -\gamma U(z_1,t_j) + U(z_2,t_j) + \gamma u,$$
$$U(z_{N+2},t_j) = U(z_N,t_j) \tag{4}$$

where $\gamma = 2v\Delta z/D$. Sorting and combining terms in Eq. (3) yields

$$\begin{aligned} U(z_i,t_{j+1}) &= (\alpha+\beta)U(z_{i-1},t_j) + (1-2\beta)U(z_i,t_j) \\ &\quad + (\beta-\alpha)U(z_{i+1},t_j), \quad i = 2,\ldots,N; \\ U(z_1,t_{j+1}) &= [1-2\beta-(\alpha+\beta)\gamma]U(z_1,t_j) + 2\beta U(z_2,t_j) \\ &\quad + [(\alpha+\beta)\gamma]u; \\ U(z_{N+1},t_{j+1}) &= 2\beta U(z_N,t_j) + (1-2\beta)U(z_{N+1},t_j) \end{aligned} \tag{5}$$

where $\alpha = (v\Delta t)/(2\Delta z)$ and $\beta = (D\Delta t)/(\Delta z)^2$.

Let $\boldsymbol{x}(k) = [U(z_1,t_k), U(z_2,t_k), \ldots, U(z_N,t_k)]^{\mathrm{T}}$, $\boldsymbol{b} = [(\alpha+\beta)\gamma, 0, \ldots, 0]^{\mathrm{T}}$, $\boldsymbol{c} = [0,0,\ldots,1]^{\mathrm{T}}$, $y(k) = U(z_{N+1},t_k)$ and

$$\boldsymbol{A} = \begin{bmatrix} k_1 & 2\beta & & & & \\ \alpha+\beta & 1-2\beta & \beta-\alpha & & & \\ & \ddots & \ddots & \ddots & & \\ & & \alpha+\beta & 1-2\beta & \beta-\alpha & \\ & & & 2\beta & 1-2\beta & \end{bmatrix}$$

where $k_1 = 1-2\beta-(\alpha+\beta)\gamma$, the system of Eq. (5) can be converted to the following discrete-time state-space form:

$$\boldsymbol{x}(k+1) = \boldsymbol{A}\boldsymbol{x}(k) + \boldsymbol{b}u(k), \quad y(k) = \boldsymbol{c}\boldsymbol{x}(k) \tag{6}$$

Because $\boldsymbol{A}$ is a high-dimensional sparse matrix and $\boldsymbol{b}$ is a high-dimensional sparse vector, a large amount of computational cost might be needed to carry out controller design and subsequent real-time implementation on the basis of the model of Eq. (6). To circumvent this problem, the Galerkin projection is applied on the discrete-time high-dimensional state-space model of Eq. (6) to derive a reduced-order model (see, for example, Wilcox & Peraire, 2002). First, we define the ensemble of $U(z,t)$ except for the points on the boundaries using the snapshots generated by the open-loop simulation of Eq. (6)(Sirovich, 1987):

$$\boldsymbol{U} := \begin{bmatrix} U(z_1,t_1) & U(z_1,t_2) & \cdots & U(z_1,t_K) \\ U(z_2,t_1) & U(z_2,t_2) & \cdots & U(z_2,t_K) \\ \vdots & \vdots & & \vdots \\ U(z_{N+1},t_1) & U(z_{N+1},t_2) & \cdots & U(z_{N+1},t_K) \end{bmatrix}$$

A singular value decomposition (SVD) of $\boldsymbol{U}$ yields that $\boldsymbol{U} = \sum_{i=1}^{K}\boldsymbol{\phi}_i\lambda_i\boldsymbol{\psi}_i^{\mathrm{T}}$, where

$$\boldsymbol{\phi}_i^{\mathrm{T}}\boldsymbol{\phi}_j = \begin{cases} 0, & i \neq j \\ 1, & i = j \end{cases} \quad \text{and} \quad \lambda_1 \geq \lambda_2 \geq \cdots \geq 0$$

Let $\boldsymbol{\Phi}$ ($\boldsymbol{\Phi} = [\boldsymbol{\phi}_1, \boldsymbol{\phi}_2, \ldots, \boldsymbol{\phi}_r]$) be the matrix composed by empirical eigenfunctions ($\boldsymbol{\phi}_i$) corresponding to the first r singular values of matrix composed by the ensemble of $\boldsymbol{U}$, it can be shown that $\boldsymbol{x}(k) \approx \boldsymbol{\Phi}\boldsymbol{a}(k)$, and $\boldsymbol{a}(k) \approx \boldsymbol{\Phi}^{\mathrm{T}}\boldsymbol{x}(k)$. Therefore, Eq. (6) can be converted to the following form:

$$\boldsymbol{\Phi}^{\mathrm{T}}\boldsymbol{\Phi}\boldsymbol{a}(k+1) = \boldsymbol{\Phi}^{\mathrm{T}}\boldsymbol{A}\boldsymbol{\Phi}\boldsymbol{a}(k) + \boldsymbol{\Phi}^{\mathrm{T}}\boldsymbol{b}u(k), \quad y(k) = \boldsymbol{c}\boldsymbol{\Phi}\boldsymbol{a}(k) \tag{7}$$

Note that $\boldsymbol{\Phi}^{\mathrm{T}}\boldsymbol{\Phi} = \boldsymbol{I}$ is an identity matrix. By construction, a reduced-order discrete-time model can be derived as

$$\boldsymbol{a}(k+1) = \boldsymbol{A}_r\boldsymbol{a}(k) + \boldsymbol{b}_r u(k), \quad y(k) = \boldsymbol{c}_r\boldsymbol{a}(k) \tag{8}$$

where $\boldsymbol{A}_r = \boldsymbol{\Phi}^{\mathrm{T}}\boldsymbol{A}\boldsymbol{\Phi}$, $\boldsymbol{b}_r = \boldsymbol{\Phi}^{\mathrm{T}}\boldsymbol{b}$, and $\boldsymbol{c}_r = \boldsymbol{c}\boldsymbol{\Phi}$.

As a result, the $(N+1)$st order state-space model is reduced to an r th order model through the Galerkin projection; this reduced-order model will be used for controller design and real-time implementation. The accuracy of the reduced-order model increases with its dimension, however, the computational cost increases accordingly. In practice, the order of the reduced-order model is chosen such that at least 99.5% of the energy embedded in the ensemble of the state variable of Eq. (6) is captured by the empirical eigenfunctions.

The optimal control problem represented by Eq. (2), if written in terms of the discretized model of Eq. (8), takes the form

$$\min_{\tilde{u}} J = \sum_{n=1}^{\infty}(\tilde{\boldsymbol{a}}^{\mathrm{T}}\boldsymbol{Q}\tilde{\boldsymbol{a}} + \tilde{u}^{\mathrm{T}}R\tilde{u}) \tag{9}$$

where $\boldsymbol{Q} = \boldsymbol{c}_r^{\mathrm{T}}\boldsymbol{c}_r = \boldsymbol{\Phi}^{\mathrm{T}}\boldsymbol{c}^{\mathrm{T}}\boldsymbol{c}\boldsymbol{\Phi}$, $R = \epsilon^2$, and the tilde sign stands for the deviation of the variable from its steady-state value. The solution of this LQR problem is given by the state feedback law: $\tilde{\boldsymbol{u}} = -\boldsymbol{K}\tilde{\boldsymbol{a}}$, where $\boldsymbol{K} = (\boldsymbol{b}_r^{\mathrm{T}}\boldsymbol{S}\boldsymbol{b}_r + R)^{-1}(\boldsymbol{b}_r^{\mathrm{T}}\boldsymbol{S}\boldsymbol{A}_r)$, and $\boldsymbol{S}$ is determined by the discrete-time Riccati equation (Arnold & Laub, 1984):

$$\boldsymbol{A}_r^{\mathrm{T}}\boldsymbol{S}\boldsymbol{A}_r - \boldsymbol{S} - (\boldsymbol{A}_r^{\mathrm{T}}\boldsymbol{S}\boldsymbol{b}_r)(\boldsymbol{b}_r^{\mathrm{T}}\boldsymbol{S}\boldsymbol{b}_r + R)^{-1}(\boldsymbol{b}_r^{\mathrm{T}}\boldsymbol{S}\boldsymbol{A}_r) + \boldsymbol{Q} = 0 \tag{10}$$

Remark 1. In the present work, an explicit scheme is used for both the temporal and spatial discretization. When an implicit or semi-implicit scheme is used to improve the numerical stability

Table 1
Parameters used in the simulation of the diffusion-convection process

v	0.5
l	1
D	0.01
N	200
t_f	4
Δz	0.005
Δt	0.001

of the algorithm, the state-space model will be of the following form:

$$\boldsymbol{A}_1\boldsymbol{x}(k+1) = \boldsymbol{A}_2\boldsymbol{x}(k) + \boldsymbol{b}u(k), \quad y(k) = \boldsymbol{c}\boldsymbol{x}(k) \tag{11}$$

where $\boldsymbol{A}_1$ and $\boldsymbol{A}_2$ are sparse matrices. The optimal control design can proceed in a similar fashion on the basis of the model of Eq. (11).

Remark 2. The proposed method might be extended to other numerical schemes, such as the finite volume method used in the computational fluid dynamics. However, further development is needed for this approach to be extended to PDEs that are nonlinear. In the subsequent section, we will discuss the control of a PDE with nonlinear terms (e.g. reactions of second order) using orthogonal collocation.

2.3. Results and discussion

2.3.1. Open-loop simulations

The open-loop simulations (with $u(t) \equiv 1$) are made using the parameters listed in Table 1. The spatiotemporal profile of the concentration is shown in Fig. 1. Note that since the Robin (mixed) boundary condition is applied at the entrance of the reactor, the concentration at $z = 0^+$ is not fixed at 1. Instead, it takes a time period ($\Delta t = 0.6$) for the concentration at the inlet to reach its steady-state value. Moreover, the concentration increases monotonically in both space and time, which is somewhat different from the dynamic behavior of the closed-loop system to be shown later in which the input varies with time.

To verify the finite difference solution of Eq. (1), we carried out a comparison of the finite difference numerical solution

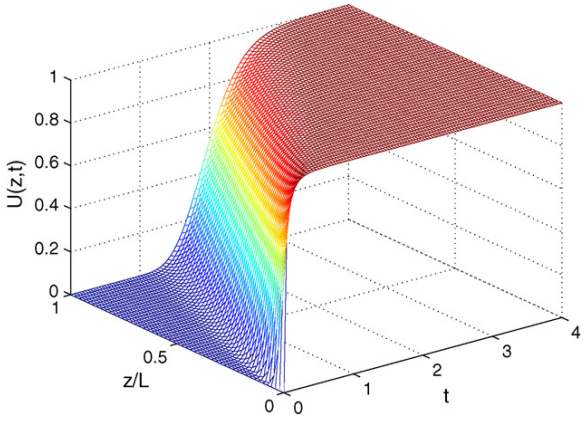

Fig. 1. Diffusion-convection process: open-loop concentration profile.

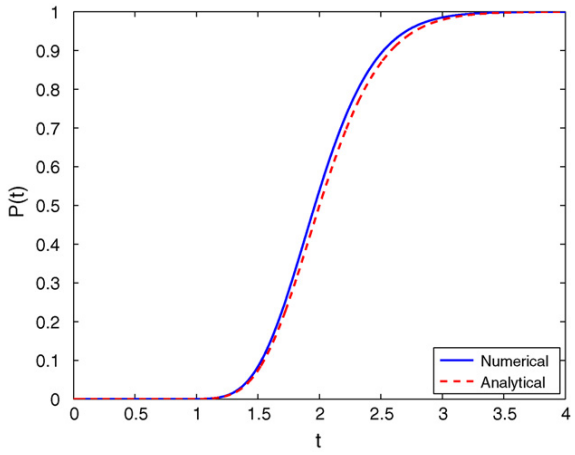

Fig. 2. Diffusion-convection process: cumulative residence time distribution solved from numerical simulation of a high-dimensional state-space model and an analytic solution with approximate boundary conditions.

with an analytic solution in which the boundary conditions are slightly modified. It has been shown that Eq. (1) can be solved analytically with the following boundary conditions: $U(\psi = -\infty) = 1$ and $U(\psi = \infty) = 0$, where $\psi = (z - vt)/(\sqrt{4Dt})$ (see, for example, Rawlings & Ekerdt, 2002). Specifically, the original PDE of Eq. (1) with these boundary conditions can be converted to an ODE of the form:

$$\frac{\mathrm{d}^2U}{\mathrm{d}\psi^2} + 2\psi\frac{\mathrm{d}U}{\mathrm{d}\psi} = 0 \tag{12}$$

If the original boundary conditions are approximated by $U(\psi = -\infty) = 1$ and $U(\psi = \infty) = 0$, an analytic solution can be obtained as follows:

$$U(\psi) = \frac{1}{2}\,\mathrm{erfc}(\psi) \tag{13}$$

where $\mathrm{erfc}(\psi)$ is the complementary error function defined by $\mathrm{erfc}(\psi) = 1 - (2)/(\sqrt{\pi})\int_0^{\psi} \mathrm{e}^{-t^2}\,\mathrm{d}t$. The cumulative residence time distribution with these approximate boundary conditions is then derived as

$$P(t) = \frac{U(L,t)}{1} = \frac{1}{2}\,\mathrm{erfc}\left(\frac{L - vt}{\sqrt{4Dt}}\right) \tag{14}$$

A comparison of the cumulative residence time distribution (a function that connects the input and output from a viewpoint of process control) solved by the numerical method and the analytical method with approximate boundary conditions is shown in Fig. 2. It can be seen that these two approaches yield almost the same result despite some minor difference when the step change passes through the outlet.

We now turn to the computation of a reduced-order model suitable for optimal controller design and implementation. First, the SVD is applied to an ensemble of the open-loop solutions of the state variable $\boldsymbol{x}$ and 4001 snapshot profiles are used. Therefore, the matrix is 201×4001. The singular values are sorted in a descending order and the normalized cumulative sum of eigenvalues ($\sum_{i=1}^{r}\lambda_i/\sum_{i=1}^{\infty}\lambda_i$) is shown in Fig. 3. It is seen that 69%

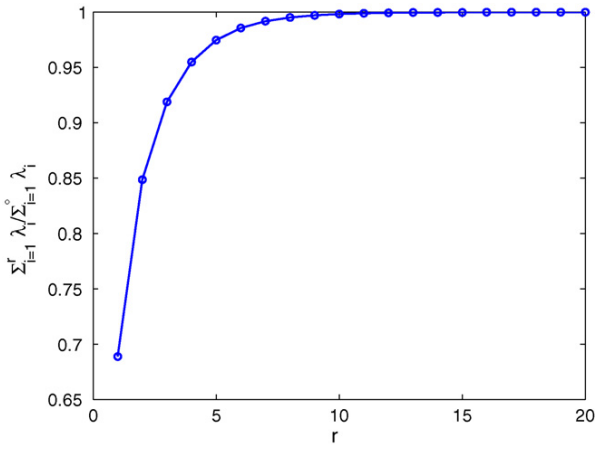

Fig. 3. Diffusion-convection process: cumulative sum of eigenvalues for ensemble constructed from the high-dimensional model.

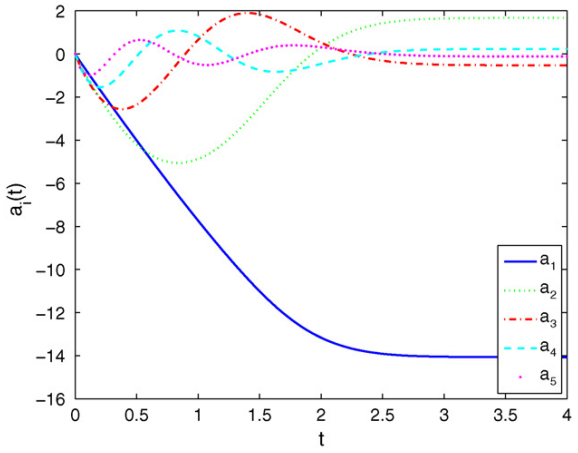

Fig. 5. Diffusion-convection process: evolution of the first five Fourier coefficients in the open-loop system.

of the energy of the ensemble of $\boldsymbol{x}$ is embedded in the first eigenfunction, 16% in the second eigenfunction, and so on. Further, the first 10 eigenfunctions capture 99.8% of the ensemble energy ($\sum_{i=1}^{\infty}\lambda_i$). If the number of eigenfunctions increases to 15 or to 30, the amount of energy captured is 99.98% or 99.99998%, respectively. Therefore, by applying the Galerkin projection to the PDE model, we can derive a 10–30th order state-space model to capture the dominant process characteristics of the original 201st order state-space model with very reasonable accuracy.

The first five eigenfunctions corresponding to the five largest eigenvalues are shown in Fig. 4. It can be easily seen that $\phi_i(z)$ crosses the horizontal axis $i-1$times, or it has $i-1$ zeros. For example, the first eigenfunction has no zero, the second one has one zero, and the third one has two zeros and so on. The evolution of the Fourier coefficients a_i corresponding to the first five eigenfunctions is shown in Fig. 5. Also, $a_i(t)$ has $i-1$ local maxima or minima (excluding the final stabilized value). Moreover, the norm of $a_i(t)$ decreases gradually as i increases, which is consistent with the magnitude of the eigenvalues. When the process approaches to its steady state, all the coefficients become constants.

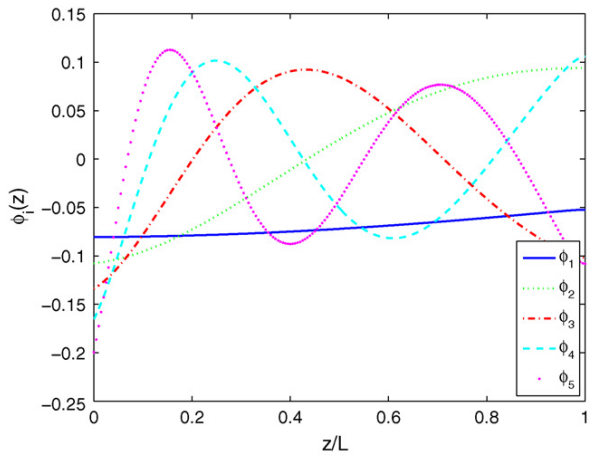

Fig. 4. Diffusion-convection process: first five empirical eigenfunctions for ensemble constructed from the high-dimensional model.

The deviation of the spatiotemporal profile of the concentration in the open-loop system obtained by the reduced-order models with $r = 10$, 15, and 30 from the one using the high-order model is shown in Fig. 6. It is seen that the largest deviations occur near the inlet of the reactor at time close to zero. This is an inevitable behavior of a series solution to a PDE. As time increases, the deviation tends to decrease and the series solution is closer to the actual solution. Furthermore, a more accurate description of the concentration profile can be described by using more eigenfunctions, which is explained by $|U_{\text{red}} - U| = \sum_{i=r+1}^{\infty}|\phi_i\lambda_i\psi_i^{\text{T}}| = \sum_{i=r+1}^{\infty}\lambda_i$.

2.3.2. *Closed-loop simulations*

The design of the optimal controllers is based on the reduced-order models and the control actions are applied to the high-order approximation of the process. In all closed-loop simulations, the weight on the control action (R) is set to be 0.25. The optimal profiles of manipulated input based on reduced-order models of different dimensions and the controlled output from the high-dimensional model are shown in Figs. 7 and 8. It is seen that the optimal trajectories of the input variable and the output variable are almost identical between $r = 10$, 15 and 30. Different from the open-loop system, where a steady increase in the output concentration can be observed, the output concentration in the closed-loop system oscillates and reaches one peak and one valley before it stabilizes at one. The input concentration also oscillates before it reaches a constant value.

The deviation of the spatiotemporal concentration profile in the closed-loop system obtained using the reduced-order models from the one using the high-order model with the same control action is shown in Fig. 9. As compared to those in the open-loop system, the deviation of the reduced-order model from the high-order model is larger but still within an acceptable range. A smaller deviation is expected when more empirical eigenfunctions are used in the reduced-order model.

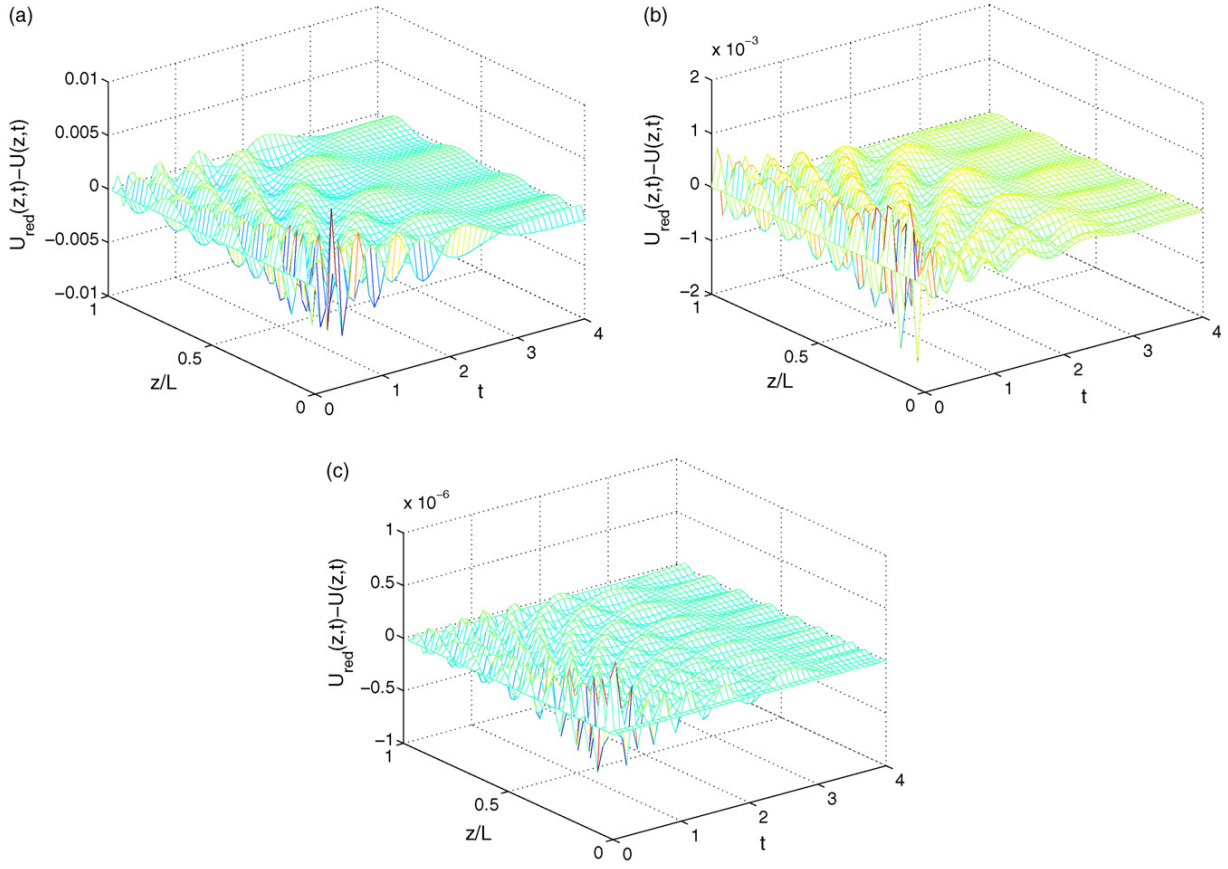

Fig. 6. Diffusion-convection process: deviation of the open-loop concentration profile calculated from the reduced-order models from the high-order model (a, $r = 10$; b, $r = 15$; c, $r = 30$).

The spatiotemporal profile of the concentration in the closed-loop system with control action calculated from a 30th order model is shown in Fig. 10. Different from the one in the open-loop system, the concentration profile is more skewed. Although the concentration is continuously decreasing from the inlet of the reactor to the outlet in the beginning, the concentration in the middle of the reactor might be larger than the one at the inlet during the transition process, or the diffusion flux is in the opposite direction of the convection. Based on the closed-loop concentration profile, the evolution of the first five Fourier

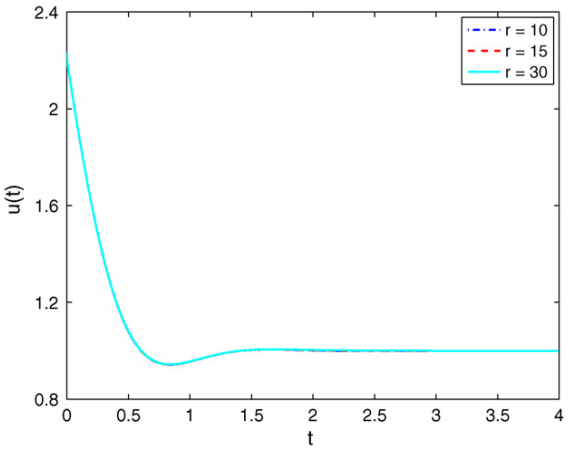

Fig. 7. Diffusion-convection process: manipulated input profile—controller designed on the basis of the reduced-order model with different number of basis functions.

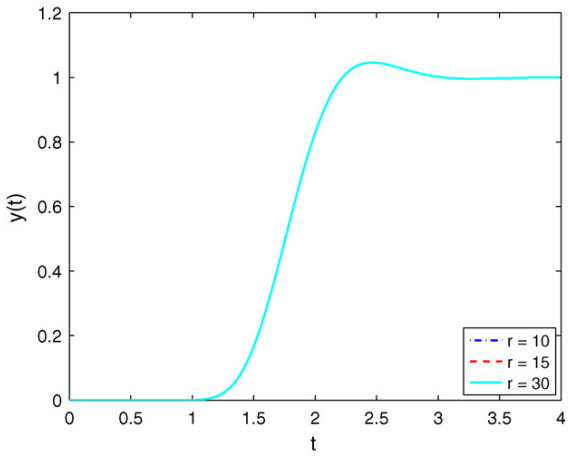

Fig. 8. Diffusion-convection process: controlled output from the high-dimensional state-space model based on the control action calculated on the basis of the reduced-order models.

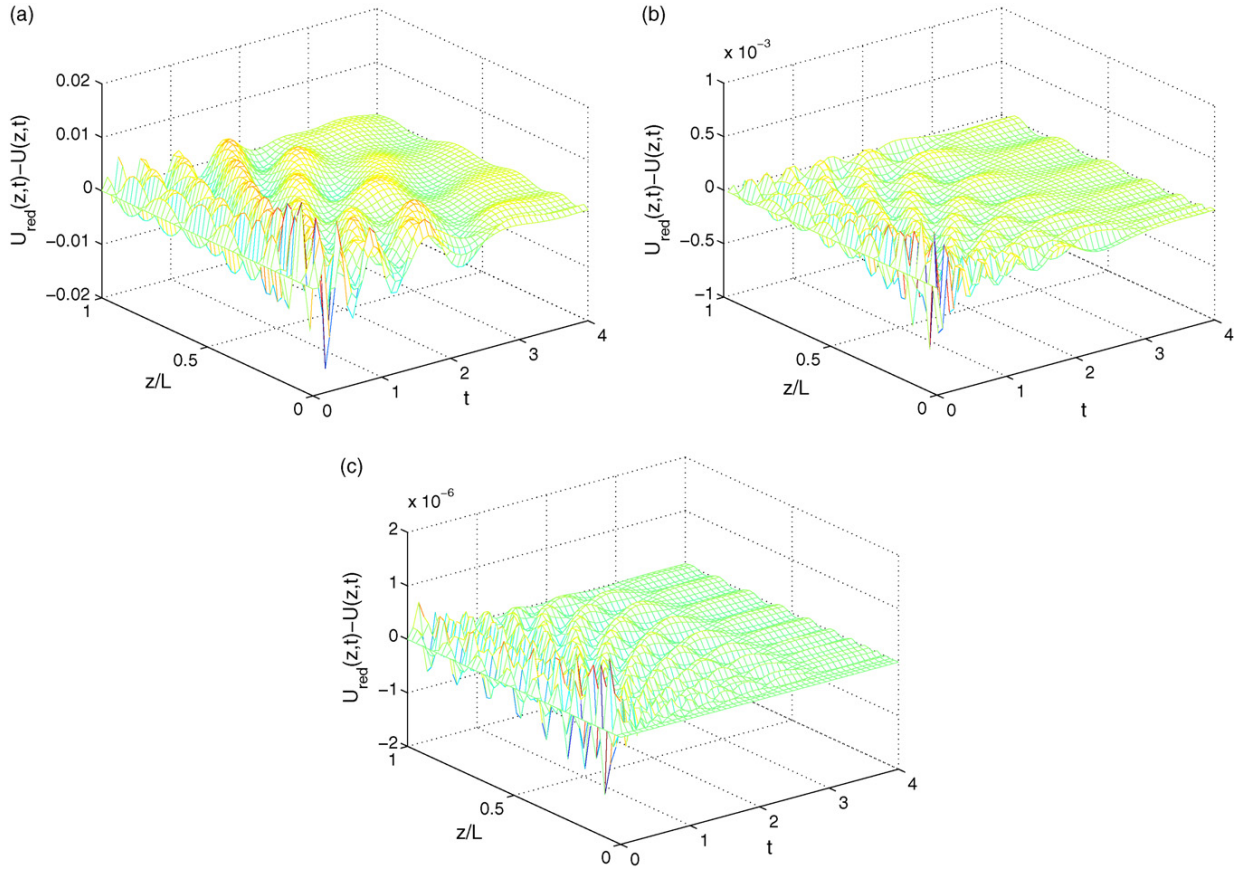

Fig. 9. Diffusion-convection process: deviation of the concentration profile derived from the reduced-order models from the high-dimensional model with the same control action in the closed-loop system (a, $r = 10$; b, $r = 15$; c, $r = 30$).

coefficients is calculated and is shown in Fig. 11. Compared to the one in the open-loop system, the norm of a_i in the closed-loop system is larger, but it reaches its steady-state in a shorter time.

Remark 3. In a previous work (Li & Christofides, 2007), we proposed an input/output approach to the optimal control of concentration transition in distributed chemical reactors with input constraints. The control problem was formulated as the one of minimizing the following functional:

$$\min_{u(t)} J = \int_0^\infty (y(t) - y_f)^2 \, \mathrm{d}t + \epsilon^2 \int_0^\infty (u(t) - u_f)^2 \, \mathrm{d}t,$$
$$\text{s.t.} \quad u_{\min} \leq u(t) \leq u_{\max} \tag{15}$$

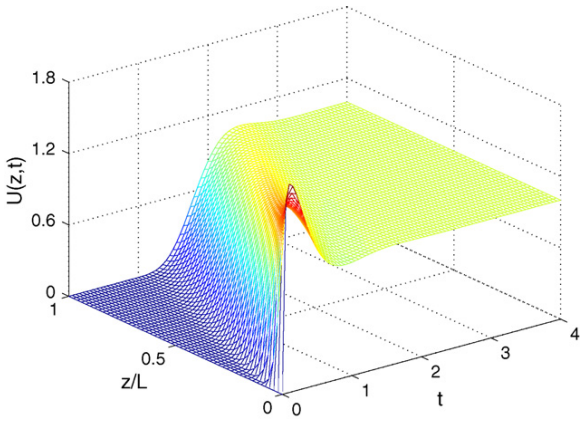

Fig. 10. Diffusion-convection process: concentration profile in the closed-loop system with control action calculated from a 30th order model.

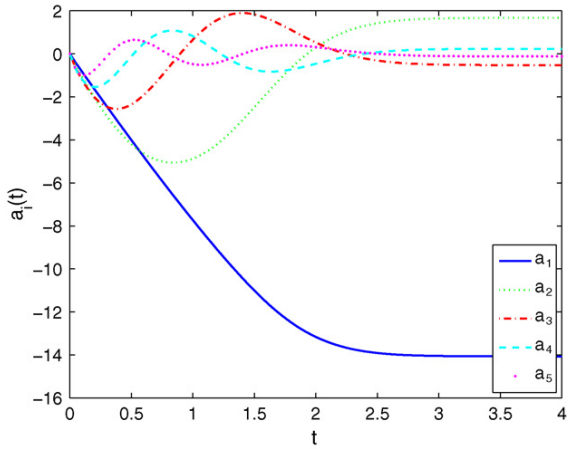

Fig. 11. Diffusion-convection process: evolution of the first five Fourier coefficients in the closed-loop system.

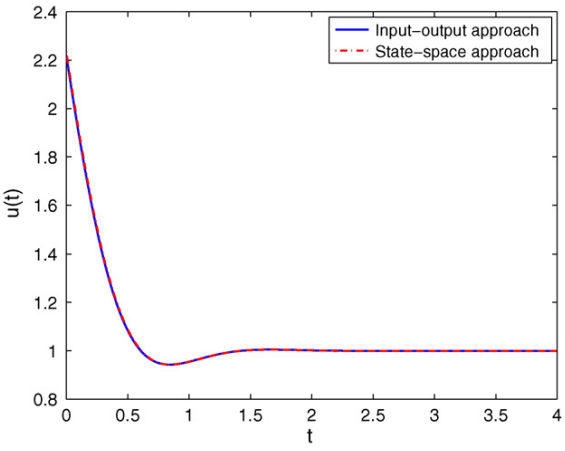

Fig. 12. Diffusion-convection process: optimal trajectory of manipulated input solved using the input/output approach and the state-space approach.

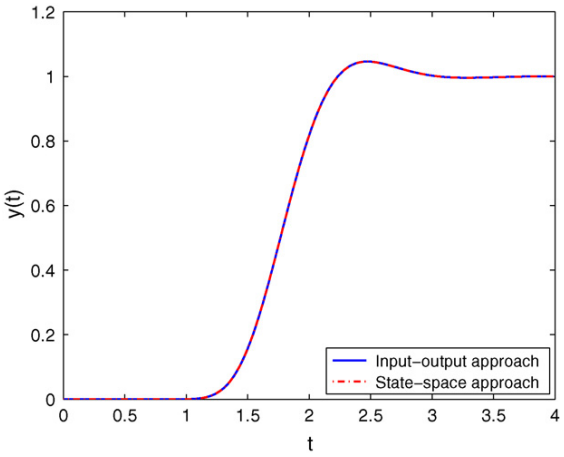

Fig. 13. Diffusion-convection process: optimal trajectory of controlled output solved using the input/output approach and the state-space approach.

where $y_f = u_f = 1$ is the target concentration of the input and output at the steady state, and $\epsilon = 0.5$ to match the cost function in the current work. It has been shown that this problem can be converted to an equivalent least square minimization problem of the form (Li & Christofides, 2007):

$$\min_{\boldsymbol{u}} J = ||\boldsymbol{A}\boldsymbol{u} - \boldsymbol{b}||^2, \quad \text{s.t.} \quad u_{\min} \le u(t) \le u_{\max} \tag{16}$$

where $\boldsymbol{A} = \begin{bmatrix} \boldsymbol{\Delta P} \\ \epsilon \boldsymbol{I} \end{bmatrix}$, $\boldsymbol{b} = \begin{bmatrix} \boldsymbol{e} \\ \epsilon \boldsymbol{e} \end{bmatrix}$, $\boldsymbol{e} = [\,1 \quad 1 \quad \dots \quad 1\,]^{\mathrm{T}}$, and

$$\boldsymbol{\Delta P} = \begin{bmatrix} P_1 & 0 & \dots & \dots & 0 \\ P_2 - P_1 & P_1 & \ddots & & \vdots \\ \vdots & \ddots & \ddots & \ddots & \vdots \\ \vdots & & \ddots & P_1 & 0 \\ P_k - P_{k-1} & \dots & \dots & P_2 - P_1 & P_1 \end{bmatrix} \tag{17}$$

with $P_i = P(i\Delta t)$ is the cumulative residence time distribution at $t = i\Delta t$. The final time $t_f = k\Delta t$ is chosen such that a near steady state has been reached at t_f in the closed-loop system. The same optimal control problem is solved by both the state-space approach and the input/output approach and the results are shown in Figs. 12 and 13. It is seen that the input/output approach based on the concept of residence time distribution derived from the high-order model and the state-space approach based on the reduced-order model ($r = 30$) derived from the Galerkin projection with empirical eigenfunctions as basis functions yield the same optimal control trajectory.

3. Optimal control of diffusion-convection-reaction processes

3.1. Process model and spatial discretization

Consider an isothermal dispersed tubular chemical reactor with simultaneous convection, diffusion and a generic reaction. The evolution of concentration is described by the following PDE subject to the so-called Danckwerts boundary conditions (Danckwerts, 1953):

$$\frac{\partial U(z,t)}{\partial t} = -v\frac{\partial U(z,t)}{\partial z} + D\frac{\partial^2 U(z,t)}{\partial z^2} + R_a(U(z,t)), \quad \text{s.t.}$$
$$vU(0^-,t) = vU(0^+,t) - D\left.\frac{\partial U(z,t)}{\partial z}\right|_{z=0^+}, \quad \left.\frac{\partial U(z,t)}{\partial z}\right|_{z=L} = 0 \tag{18}$$

where $U(0^-,t) = u(t)$ is the input variable, $U(L,t) = y(t)$ the output variable and $R_a(z,t)$ is the reaction term.

We solve the model of Eq. (18) using orthogonal collocation. By applying the orthogonal collocation on N finite elements within the spatial domain, the primary variable $U(z,t)$ can be expressed as $U(z,t) = \sum_{i=1}^{N} l_i(z)U(z_i,t)$ at time t, where $l_i(z)$ is the Lagrange interpolation polynomial of $(N-1)$ th order:

$$l_i(z) = \prod_{j=1, j\neq i}^{N} \frac{z - z_j}{z_i - z_j} \tag{19}$$

which satisfies

$$l_i(z_j) = \begin{cases} 0, & i \neq j \\ 1, & i = j \end{cases} \tag{20}$$

Another important property of the Lagrange interpolation polynomials used in the orthogonal collocation approach is that they are orthogonal to each other, i.e.

$$\int_0^1 l_i(z)l_j(z)\,\mathrm{d}z = \begin{cases} 0, & i \neq j \\ 1, & i = j \end{cases} \tag{21}$$

Therefore, a small number of collocation points are required to obtain an accurate solution.

Based on the orthogonal collocation scheme, the collocation elements (z_i) and the Lagrange interpolation polynomial can be determined a priori without information from the structure of the PDE. Therefore, the partial derivatives of U with respect to

the spatial coordinate can be expressed as follows:

$$\frac{\partial U(z,t)}{\partial z} = \sum_{i=1}^{N} U(z_i,t)\frac{\mathrm{d}l_i(z)}{\mathrm{d}z} \tag{22}$$

$$\frac{\partial U^2(z,t)}{\partial z^2} = \sum_{i=1}^{N} U(z_i,t)\frac{\mathrm{d}^2 l_i(z)}{\mathrm{d}z^2} \tag{23}$$

Defining the two matrices:

$$\boldsymbol{A} = \left\{ A_{i,j} = \frac{\mathrm{d}l_j(z_i)}{\mathrm{d}z};\quad i,j = 1,2,\ldots,N \right\} \tag{24}$$

and

$$\boldsymbol{B} = \left\{ B_{i,j} = \frac{\mathrm{d}l_j^2(z_i)}{\mathrm{d}z^2};\quad i,j = 1,2,\ldots,N \right\} \tag{25}$$

the original PDE of Eq. (18) can be converted to a set of ODEs:

$$\begin{aligned}
\frac{\mathrm{d}U(z_2,t)}{\mathrm{d}t} &= -v\sum_{j=1}^{N} A_{2,j}U(z_j,t) + D\sum_{j=1}^{N} B_{2,j}U(z_j,t) \\
&\quad + R_a(U(z_2,t)) \\
&\vdots \\
\frac{\mathrm{d}U(z_{N-1},t)}{\mathrm{d}t} &= -v\sum_{j=1}^{N} A_{N-1,j}U(z_j,t) \\
&\quad + D\sum_{j=1}^{N} B_{N-1,j}U(z_j,t) + R_a(U(z_{N-1},t))
\end{aligned} \tag{26}$$

subject to the following boundary conditions:

$$vu(t) = vU(z_1,t) - D\sum_{j=1}^{N} A_{1,j}U(z_j,t),$$

$$\sum_{j=1}^{N} A_{N,j}U(z_j,t) = 0 \tag{27}$$

The system of Eqs. (26)–(27) is a DAE of index one which can be further simplified by incorporating the boundary conditions into the ordinary differential equation. First, we rewrite the equations describing the boundary conditions in the following form:

$$\begin{aligned}
&(v - DA_{1,1})U(z_1,t) - DA_{1,N}U(z_N,t) \\
&\quad = D\sum_{j=2}^{N-2} A_{1,j}U(z_j,t) + vu(t),
\end{aligned}$$

$$A_{N,1}U(z_1,t) + A_{N,N}U(z_N,t) = -\sum_{j=2}^{N-2} A_{N,j}U(z_j,t) \tag{28}$$

and then define the following matrices and vectors:

$$\boldsymbol{A_d} = \{A_{r_{i,j}} = A_{i+1,j+1};\quad i,j = 1,2,\ldots,N-2\},$$

$$\boldsymbol{B_d} = \{B_{r_{i,j}} = B_{i+1,j+1};\quad i,j = 1,2,\ldots,N-2\},$$

$$\boldsymbol{A_b} = \begin{bmatrix} A_{2,1} & A_{2,N} \\ \vdots & \vdots \\ A_{N-1,1} & A_{N-1,N} \end{bmatrix},\quad \boldsymbol{B_b} = \begin{bmatrix} B_{2,1} & B_{2,N} \\ \vdots & \vdots \\ B_{N-1,1} & B_{N-1,N} \end{bmatrix},$$

$$\boldsymbol{M} = \begin{bmatrix} v - DA_{1,1} & -DA_{1,N} \\ A_{N,1} & A_{N,N} \end{bmatrix},\quad \boldsymbol{V} = \begin{bmatrix} v \\ 0 \end{bmatrix},$$

$$\boldsymbol{N} = \begin{bmatrix} DA_{1,2} & \cdots & DA_{1,N-1} \\ -A_{N,2} & \cdots & -A_{N,N-1} \end{bmatrix},\quad \boldsymbol{H} = [0 \quad 1],$$

$$\boldsymbol{x} = [U(z_2,t)\ \ U(z_3,t)\ \ \cdots\ \ U(z_{N-1},t)]^{\mathrm{T}},$$

$$\boldsymbol{d} = [U(z_1,t)\ \ U(z_N,t)]^{\mathrm{T}},$$

$$\boldsymbol{f} = [R_a(U(z_2,t))\ \ R_a(U(z_3,t))\ \ \cdots\ \ R_a(U(z_{N-1},t))]^{\mathrm{T}} \tag{29}$$

Using the above definitions, we have that

$$\boldsymbol{d} = \boldsymbol{M}^{-1}\boldsymbol{N}\boldsymbol{x} + \boldsymbol{M}^{-1}\boldsymbol{V}u \tag{30}$$

provided that $\boldsymbol{M}$ is nonsingular. Using the above notation, Eqs. (26)–(27) can be then written as

$$\begin{aligned}
\dot{\boldsymbol{x}} &= (-v\boldsymbol{A_d} + D\boldsymbol{B_d})\boldsymbol{x} + (-v\boldsymbol{A_b} + D\boldsymbol{B_b})\boldsymbol{d} + \boldsymbol{f}(\boldsymbol{x}) \\
&= [(-v\boldsymbol{A_d} + D\boldsymbol{B_d}) + (-v\boldsymbol{A_b} + D\boldsymbol{B_b})\boldsymbol{M}^{-1}\boldsymbol{N}]\boldsymbol{x} + \boldsymbol{f}(\boldsymbol{x}) \\
&\quad + (-v\boldsymbol{A_b} + D\boldsymbol{B_b})\boldsymbol{M}^{-1}\boldsymbol{V}u
\end{aligned} \tag{31}$$

and

$$y = \boldsymbol{H}\boldsymbol{M}^{-1}\boldsymbol{N}\boldsymbol{x} + \boldsymbol{H}\boldsymbol{M}^{-1}\boldsymbol{V}u \tag{32}$$

which is in the standard state-state form of a nonlinear dynamic process:

$$\dot{\boldsymbol{x}} = \boldsymbol{A_c}\boldsymbol{x} + \boldsymbol{B_c}u + \boldsymbol{f}(\boldsymbol{x}),\quad y = \boldsymbol{C_c}\boldsymbol{x} + \boldsymbol{D_c}u \tag{33}$$

where $\boldsymbol{A_c} = [(-v\boldsymbol{A_d} + D\boldsymbol{B_d}) + (-v\boldsymbol{A_b} + D\boldsymbol{B_b})\boldsymbol{M}^{-1}\boldsymbol{N}]$, $\boldsymbol{B_c} = (-v\boldsymbol{A_b} + D\boldsymbol{B_b})\boldsymbol{M}^{-1}\boldsymbol{V}$, $\boldsymbol{C_c} = \boldsymbol{H}\boldsymbol{M}^{-1}\boldsymbol{N}$, $\boldsymbol{D_c} = \boldsymbol{H}\boldsymbol{M}^{-1}\boldsymbol{V}$.

3.2. Optimal control using LQR

The optimal control problem for the nonlinear ODE system of Eq. (33) can be solved using control vector parametrization or nonlinear programming of the discretized system (see, for example, Varshney & Armaou, 2006). To circumvent the computational complexity, we focus on the linearized system around the open-loop steady-state. The linearized system works as a state estimator based on which the control action is calculated. Because both the open-loop nonlinear system and the linearized system are stable, the observer gain is set to be zero for simplicity.

Let $\tilde{\boldsymbol{x}} = \boldsymbol{x} - \boldsymbol{x}_s$, $\tilde{u} = u - u_s$, and $\tilde{y} = y - y_s$, the nonlinear system can be written as follows:

$$\dot{\tilde{\boldsymbol{x}}} = \boldsymbol{A_c}\tilde{\boldsymbol{x}} + \boldsymbol{B_c}\tilde{u} + \boldsymbol{f}(\tilde{\boldsymbol{x}} + \boldsymbol{x}_s) - \boldsymbol{f}(\boldsymbol{x}_s),\quad \tilde{y} = \boldsymbol{C_c}\tilde{\boldsymbol{x}} + \boldsymbol{D_c}\tilde{u} \tag{34}$$

which can be linearized around the steady-state using the Jacobian matrix $\boldsymbol{A_l} = (\partial \boldsymbol{f}(\boldsymbol{x}))/(\partial \boldsymbol{x})|_{\boldsymbol{x}=\boldsymbol{x}_s}$ to obtain:

$$\dot{\tilde{\boldsymbol{x}}} = (\boldsymbol{A_c} + \boldsymbol{A_l})\tilde{\boldsymbol{x}} + \boldsymbol{B_c}\tilde{u},\quad \tilde{y} = \boldsymbol{C_c}\tilde{\boldsymbol{x}} + \boldsymbol{D_c}\tilde{u} \tag{35}$$

The LQR problem is to minimize the following functional:

$$\min_{u(t)} J = \int_0^\infty (\tilde{y}^2 + \epsilon^2 \tilde{u}^2)\,\mathrm{d}t \tag{36}$$

and the solution is given by the state feedback law: $\tilde{\boldsymbol{u}} = -\boldsymbol{K}\tilde{\boldsymbol{x}}$, where $\boldsymbol{K} = \boldsymbol{R}^{-1}(\boldsymbol{B}^{\mathrm{T}}\boldsymbol{S} + \boldsymbol{G}^{\mathrm{T}})$, and $\boldsymbol{S}$ is determined by the Riccati equation (Arnold & Laub, 1984):

$$(\boldsymbol{A_c} + \boldsymbol{A_l})^{\mathrm{T}}\boldsymbol{S} + \boldsymbol{S}(\boldsymbol{A_c} + \boldsymbol{A_l}) - (\boldsymbol{S}\boldsymbol{B_c} + \boldsymbol{G})\boldsymbol{R}^{-1}(\boldsymbol{B_c}^{\mathrm{T}}\boldsymbol{S} + \boldsymbol{G}^{\mathrm{T}}) + \boldsymbol{Q} = 0 \tag{37}$$

where $\boldsymbol{Q} = \boldsymbol{C_c}^{\mathrm{T}}\boldsymbol{C_c}$, $\boldsymbol{G} = \boldsymbol{C_c}^{\mathrm{T}}\boldsymbol{D_c}$, and $\boldsymbol{R} = \boldsymbol{D_c}^{\mathrm{T}}\boldsymbol{D_c} + \epsilon^2$.

Typically, the dimension of an approximate state-space model formulated using orthogonal collocation is substantially smaller than the one obtained by finite difference and can be used for controller design. Moreover, in case a large number of collocation points are needed, model reduction techniques can be used to derive a low order state-space model from the orthogonal collocation model and the controller can be synthesized using that reduced-order model. Following a similar approach presented in Section 2, Eq. (35) can be converted to the following form:

$$\dot{\tilde{\boldsymbol{a}}} = \boldsymbol{A_r}\tilde{\boldsymbol{a}} + \boldsymbol{B_r}\tilde{u}, \quad \tilde{y} = \boldsymbol{C_r}\tilde{\boldsymbol{a}} + \boldsymbol{D_r}\tilde{u} \tag{38}$$

where $\boldsymbol{A_r} = \boldsymbol{\Phi}^{\mathrm{T}}(\boldsymbol{A_c} + \boldsymbol{A_l})\boldsymbol{\Phi}$, $\boldsymbol{B_r} = \boldsymbol{\Phi}^{\mathrm{T}}\boldsymbol{B_c}$, and $\boldsymbol{C_r} = \boldsymbol{C}\boldsymbol{\Phi}$, and $\boldsymbol{D_r} = \boldsymbol{D_c}$. Therefore, the $(N-2)$ nd state-space model is reduced to an r th one through the Galerkin projection, which can be then used for controller design. The solution of this LQR problem is given by the state feedback law $\tilde{\boldsymbol{u}} = -\boldsymbol{K_r}\tilde{\boldsymbol{a}}$ following a similar approach to the one presented on the basis of the high-order model.

3.3. Results and discussion

The control problem is to make an optimal transition of the concentration at the exit of the reactor from 0.2 to 0.5. The parameters used in the simulations are listed in Table 2. The reaction term is assumed to be $R_a = -2kU^2$. To determine the concentration profile within the reactor before and after transition, the steady state form of Eq. (33) is solved:

$$0 = \boldsymbol{A_c}\boldsymbol{x_s} + \boldsymbol{B_c}u_s + \boldsymbol{f}(\boldsymbol{x_s}), \quad y_s = \boldsymbol{C_c}\boldsymbol{x_s} + \boldsymbol{D_c}u_s \tag{39}$$

and the results are shown in Figs. 14 and 15. The collocation elements are not uniformly distributed along the spatial domain, as seen in Fig. 16. Instead, they are highly clustered in the region close to the boundaries. The nonlinearity of the problem can be easily verified by checking the steady-state profiles of the concentration before and after transition, which are not proportional to each other. A calculation of the input variable also shows that

Table 2
Parameters used in the simulation of the diffusion-convection-reaction process

v	0.2
L	1
D	0.02
N	50
k	0.05

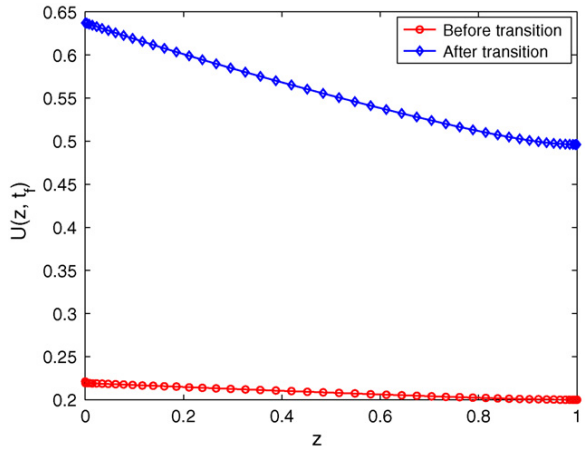

Fig. 14. Diffusion-convection-reaction process: steady-state spatial profiles of the concentration before transition and after transition.

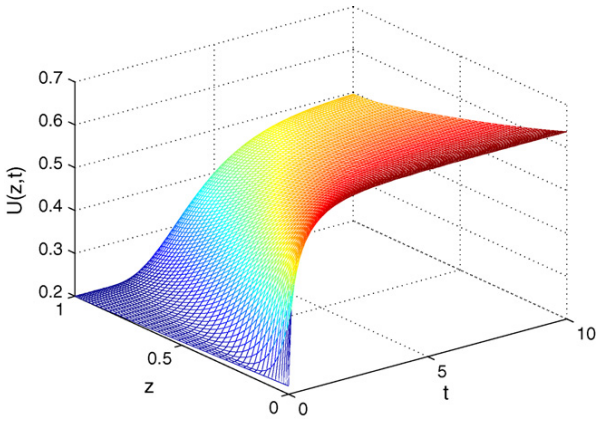

Fig. 15. Diffusion-convection-reaction process: spatiotemporal distribution of the concentration during transition in the open-loop system.

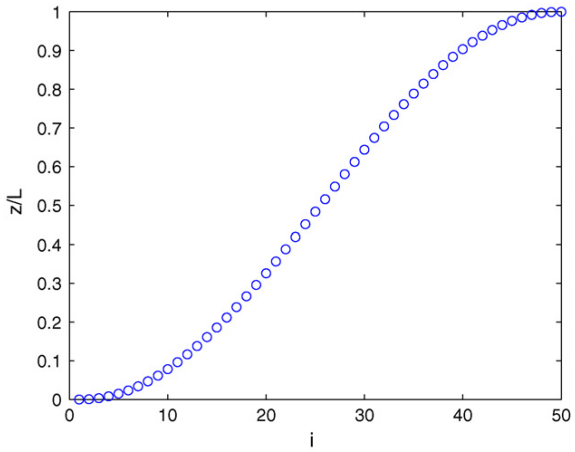

Fig. 16. Diffusion-convection-reaction process: distribution of the collocation elements in the spatial domain.

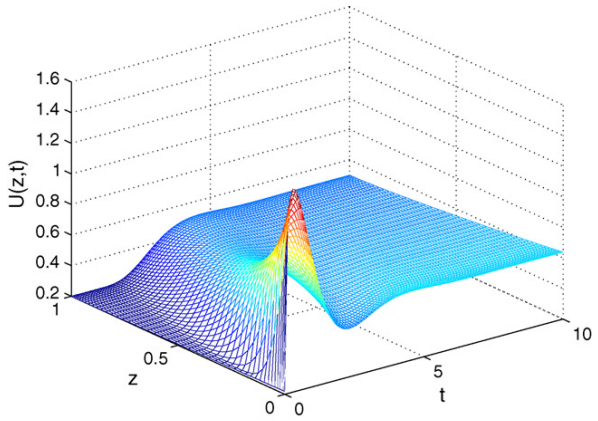

Fig. 17. Diffusion-convection-reaction process: spatiotemporal distribution of the concentration during transition in the closed-loop system.

u_s increases from 0.22 to 0.66 in order to make an increase of y_s from 0.2 to 0.5.

The closed-loop spatiotemporal profile of the concentration during the transition process solved using $\epsilon^2 = 0.01$ is shown in Fig. 17. One apparent difference between the open-loop system (Fig. 15) and the closed-loop system (Fig. 17) is that the concentration at the inlet of the reactor is not increasing all the time under optimal control. Instead, it increases initially and then decreases after reaching a peak. This behavior is very similar to the one observed for the diffusion-convection process. As we discussed before, because the original steady-state of both the original system and the linearized system is stable, the difference between these two states approaches zero as the time exceeds a certain value, which is shown in Fig. 18. The profiles of the manipulated input and of the controlled output under optimal control are shown in Figs. 19 and 20. It is seen that the transition time in the closed-loop system is significantly less than the one in the open-loop system.

In case the dimension of the finite-dimensional model formulated using the orthogonal collocation is high in order to

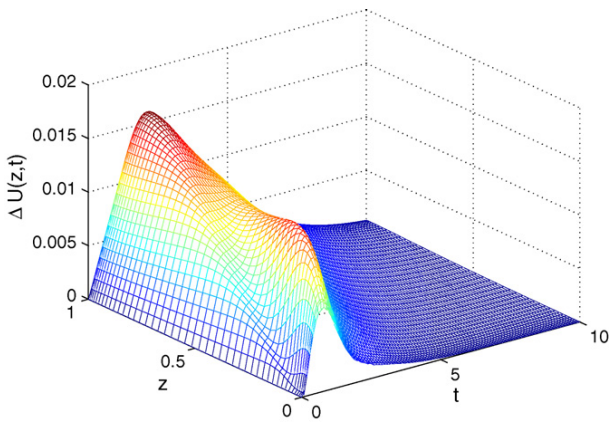

Fig. 18. Diffusion-convection-reaction process: deviation of the closed-loop concentration profile calculated from the linearized model from the nonlinear system with the same control action.

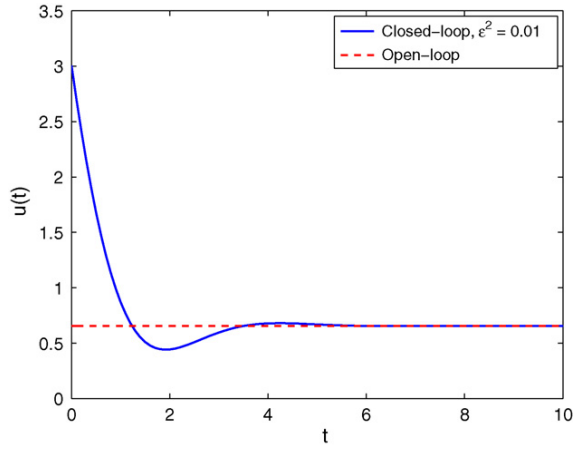

Fig. 19. Diffusion-convection-reaction process: optimal trajectory of the manipulated input based on the high-dimensional state-space model derived from orthogonal collocation.

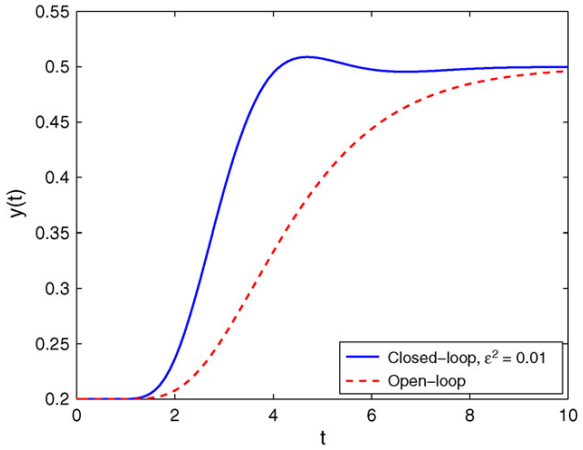

Fig. 20. Diffusion-convection-reaction process: optimal trajectory of the controlled output using optimal control action calculated on the basis of the high-dimensional state-space model derived from orthogonal collocation.

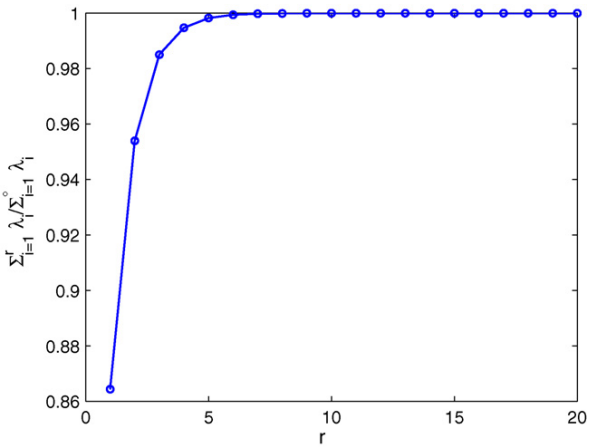

Fig. 21. Diffusion-convection-reaction process: cumulative sum of eigenvalues for ensemble constructed from the high-dimensional model.

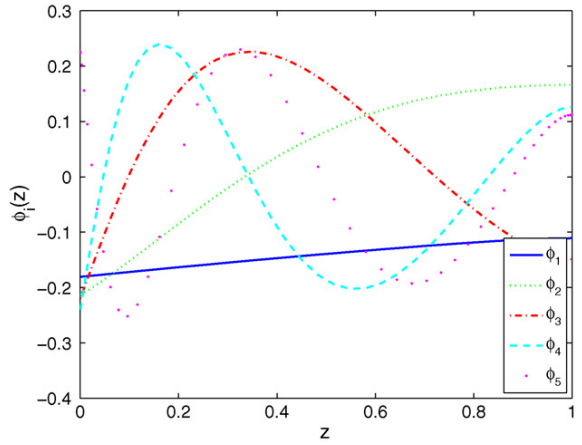

Fig. 22. Diffusion-convection-reaction process: first five empirical eigenfunctions for ensemble constructed from the high-dimensional model.

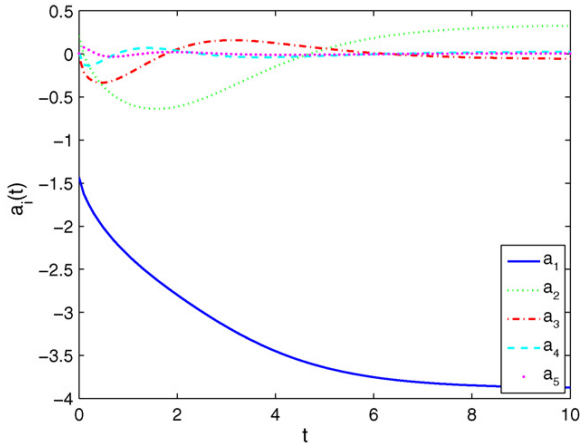

Fig. 23. Diffusion-convection-reaction process: evolution of the first five Fourier coefficients in the open-loop system.

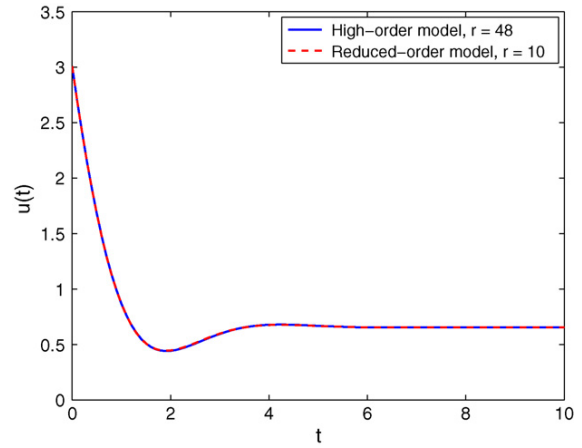

Fig. 24. Diffusion-convection-reaction process: optimal trajectory of manipulated input solved based on the reduced-order state-space model.

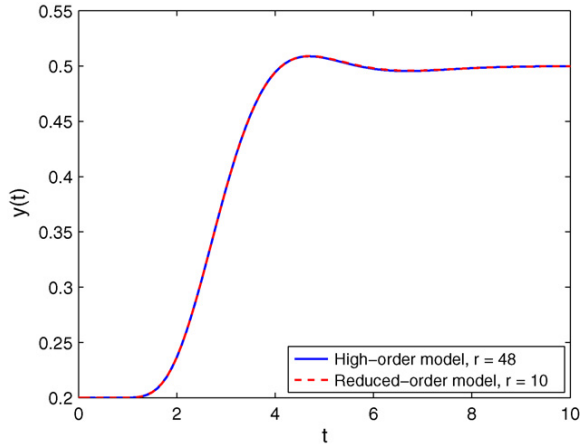

Fig. 25. Diffusion-convection-reaction process: optimal trajectory of controlled output using the control action computed on the basis of the reduced-order state-space model.

accurately describe the process, a reduced-order model might be derived using proper orthogonal decomposition techniques for controller design. Following a similar procedure used in the control of the diffusion-convection process, the SVD is first applied to an ensemble of the state variable $\boldsymbol{x}$ (a 48 $\times$ 101 matrix) to derive empirical eigenfunctions. The singular values are sorted in a descending order and the normalized cumulative sum of eigenvalues ($\sum_{i=1}^{r}\lambda_i/\sum_{i=1}^{\infty}\lambda_i$) is shown in Fig. 21. It is seen that the process can be described using about 10 empirical eigenfunctions with very reasonable accuracy. The first five eigenfunctions corresponding to the five largest eigenvalues λ_i and the evolution of the first five Fourier coefficients a_i are shown in Figs. 22 and 23. Similar to the diffusion-convection process, the magnitude of a_i decreases as i increases, which is consistent with the magnitude of the eigenvalue λ_i. The LQR problem is solved based on a 10th order model and the control action is fed to the high order nonlinear ODE model. The optimal trajectories of the manipulated input and controlled output are shown to be very close to those in which the control action is solved based on

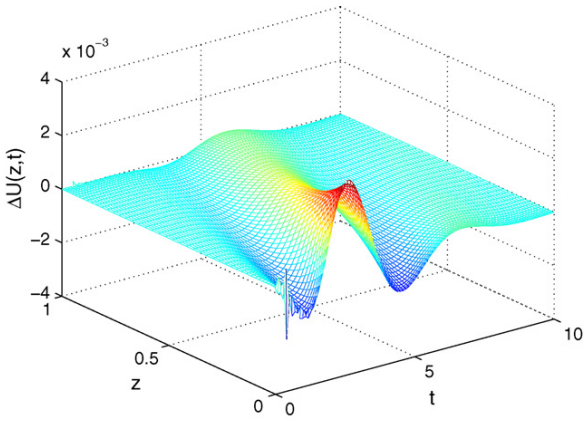

Fig. 26. Diffusion-convection-reaction process: deviation of the closed-loop spatiotemporal concentration profile calculated using the reduced-order model ($r = 10$) from the high-dimensional model ($r = 48$) with the same control action.

the high-order model (see Figs. 24 and 25). A comparison of the spatiotemporal profile of the concentration based on the control action solved using the high-order model and the reduced-order model indicates that there is some small difference in the region close to the boundary in the beginning of the transition and in the whole region during the transition. However, even such a small difference becomes negligible when the process reaches steady state (see Fig. 26).

4. Summary

We presented in this work two computationally efficient approaches for the optimal control of diffusion-convection-reaction processes described by parabolic PDEs subject to Danckwerts boundary conditions. The central idea of the proposed approaches is to construct a finite-dimensional state-space model through numerical discretization (such as finite difference and orthogonal collocation, etc.) and proper orthogonal decomposition techniques, based on which the optimal controller can be designed with affordable computational effort. The effectiveness of the proposed methods were illustrated through applications to a diffusion-convection process and a diffusion-convection-reaction process in which both the input and the output are on the boundaries.

Acknowledgement

Financial support form NSF, CTS-0325246, and start-up funding from California State Polytechnic Univerisity, Pomona (Mingheng Li), is gratefully acknowledged.

References

Ammar, A., Ryckelynck, D., Chinesta, F., & Keunings, R. (2006). On the reduction of kinetic theory models related to finitely extensible dumbbells. *Journal of Non-Newtonian Fluid Mechanics*, *134*, 136–147.

Armaou, A., & Christofides, P. D. (1999a). Nonlinear feedback control of parabolic PDE systems with time-dependent spatial domains. *Journal of Mathematical Analysis and Applications*, *239*, 124–157.

Armaou, A., & Christofides, P. D. (1999b). Plasma-enhanced chemical vapor deposition: Modeling and control. *Chemical Engineering Science*, *54*, 3305–3314.

Armaou, A., & Christofides, P. D. (2000). Wave suppression by nonlinear finite-dimensional control. *Chemical Engineering Science*, *55*, 2627–2640.

Armaou, A., & Christofides, P. D. (2002). Dynamic optimization of dissipative PDE systems using nonlinear order reduction. *Chemical Engineering Science*, *57*, 5083–5114.

Arnold, W. F., & Laub, A. J. (1984). Generalized eigenproblem algorithms and software for algebraic Riccati equations. *Proceedings of IEEE*, *72*, 1746–1754.

Baker, J., Armaou, A., & Christofides, P. D. (2000). Nonlinear control of incompressible fluid flow: Application to Burgers' equation and 2D channel flow. *Journal of Mathematical Analysis and Applications*, *252*, 230–255.

Baker, J., & Christofides, P. D. (2000). Finite dimensional approximation and control of nonlinear parabolic PDE systems. *International Journal of Control*, *73*, 439–456.

Bendersky, E., & Christofides, P. D. (2000). Optimization of transport-reaction processes using nonlinear model reduction. *Chemical Engineering Science*, *55*, 4349–4366.

Broussely, M., Bertin, Y., & Lagonotte, P. (2003). Reduction and optimisation of thermal models using Kirchhoff network theory. *International Journal of Thermal Science*, *42*, 795–804.

Cervantes, A. M., Tonelli, S., Brandolin, A., Bandoni, J. A., & Biegler, L. T. (2002). Large-scale dynamic optimization for grade transitions in a low density polyethylene plant. *Computers & Chemical Engineering*, *26*, 227–237.

Christofides, P. D. (2001). *Nonlinear and robust control of PDE systems: Methods and applications to transport-reaction processes*. Boston, USA: Birkhäuser.

Christofides, P. D., & Daoutidis, P. (1997). Finite-dimensional control of parabolic PDE systems using approximate inertial manifolds. *Journal of Mathematical Analysis and Applications*, *216*, 398–420.

Danckwerts, P. V. (1953). Continuous flow systems: Distribution of residence times. *Chemical Engineering Science*, *2*, 1–13.

Graham, W. R., Peraire, J., & Tang, K. Y. (1999). Optimal control of vortex shedding using low-order models. Part I. Open-loop model development. *International Journal of Numerical Methods in Engineering*, *44*, 945–972.

Kalkkuhl, J. C., & Doring, M. G. (1993). Modal approximation of xenon oscillations in nuclear reactors—An FEM-based approach. *Control Engineering Practice*, *1*, 791–796.

Li, M., & Christofides, P. D. (2005). Multi-scale modeling and analysis of HVOF thermal spray process. *Chemical Engineering Science*, *60*, 3649–3669.

Li, M., & Christofides, P. D. (2006). Computational study of particle in-flight behavior in the HVOF thermal spray process. *Chemical Engineering Science*, *61*, 6540–6552.

Li, M., & Christofides, P. D. (2007). An input/output approach to the optimal transition control of a class of distributed chemical reactors. *Chemical Engineering Science, 62*, 2979–2988.

Li, M., Sopko, J. F., & McCamy, J. W. (2006). Computational fluid dynamic modeling of tin oxide deposition in an impinging chemical vapor deposition reactor. *Thin Solid Films*, *155*, 1400–1410.

Lin, Y. H., & Adomaitis, R. A. (2001). Simulation and model reduction methods for an RF plasma glow discharge. *Journal of Computational Physics*, *171*, 731–752.

Liu, Y., & Jacobsen, E. W. (2004). On the use of reduced order models in bifurcation analysis of distributed parameter systems. *Computers & Chemical Engineering*, *28*, 161–169.

Lo, D. P., & Ray, W. H. (2006). Dynamic modeling of polyethylene grade transitions in fluidized bed reactors employing nickel-diimine catalysts. *Industrial & Engineering Chemical Research*, *45*, 993–1008.

McAuley, K. B., & MacGregor, J. F. (1992). Optimal grade transitions in a gas-phase polyethylene reactor. *AIChE Journal*, *38*, 1564–1576.

Park, H. M., & Jang, Y. D. (2000). Control of Burgers equation by means of mode reduction. *International Journal of Engineering Science*, *38*, 785–805.

Quarteroni, A., & Valli, A. (1997). *Numerical approximation of partial differential equations*. Berlin: Springer-Verlag.

Rawlings, J. B., & Ekerdt, J. G. (2002). *Chemical reactor analysis and design fundamentals*. Nob Hill Publishing, LLC.

Rowley, C. W., Colonius, T., & Murray, R. M. (2004). Model reduction for compressible flows using POD and Galerkin projection. *Physica D*, *189*, 115–129.

Shvartsman, S. Y., & Kevrekidis, I. G. (1998). Nonlinear model reduction for control of distributed parameter systems: A computer assisted study. *AIChE Journal*, *44*, 1579–1595.

Sirovich, L. (1987). Turbulence and the dynamics of coherent structures. Part I. Coherent structures. *Quarterly of Applied Mathematics*, *XLV*, 561–571.

Theodoropoulou, A., Adomaitis, R. A., & Zafiriou, E. (1998). Model reduction for RTCVD optimization. *IEEE Transactions on Semiconductor Manufacturing*, *11*, 85–98.

Trier, W. (1987). *Glass furnaces: Design construction & operation*. Sheffield, UK: Society of Glass Technology.

Varshney, A., & Armaou, A. (2006). Optimal operation of GaN thin film epitaxy employing control vector parametrization. *AIChE Journal*, *52*, 1378–1391.

Wilcox, K., & Peraire, J. (2002). Balanced model reduction via the proper orthogonal decomposition. *AIAA Journal*, *40*, 2323–2330.